

Measurements of Aerodynamic Performance of the Fuselage of a Hybrid Multi-Rotor Aircraft with Autorotation Capability

Zbigniew Czyż¹, Paweł Karpiński², Krzysztof Skiba², Mirosław Wendeker²

Abstract – The design and optimization of aircraft structures need to be accompanied by the analysis of their aerodynamics. This paper presents numerical calculations and wind tunnel tests to determine the aerodynamic characteristics of the designed unmanned aircraft. The aim of the study was to analyze the aerodynamic performance of the designed hybrid unmanned aerial vehicle and its longitudinal stability. This unique design, i.e. a hybrid aircraft which is a combination of a gyrocopter and a multi-rotor aircraft has not been the object of research yet. The research object is a 1:1 scale model created by the rapid prototyping method. The research was a computational and experimental study. The ANSYS Fluent software was used for the calculations, and the computational mesh of the developed model consisted of 3.5 million tetrahedral elements. The numerical investigations were carried out using the created CFD model with a $k-\omega$ turbulence submodel. In addition, the obtained results made it possible to numerically analyze the forces acting on the individual components of the research object, which is a valuable extension of the wind tunnel tests. The experimental studies were performed in a closed-loop subsonic wind tunnel. Aerodynamic forces and moments were measured using a six-component force balance. The obtained results were compared to validate the developed numerical model. The research values describe the performance of the research object in terms of minimum drag force coefficient, maximum lift to drag ratio, and properties related to stability. **Copyright © 2022 The Authors.** Published by Praise Worthy Prize S.r.l. This article is open access published under the CC BY-NC-ND license (<http://creativecommons.org/licenses/by-nc-nd/3.0/>).

Keywords: Aerodynamics, Aerodynamic Coefficient, Aircraft, Fuselage, Multirotor, Wind Tunnel

Nomenclature

CFD	Computational Fluid Dynamics
C_i	Aerodynamic force coefficient
C_{SF}	Lateral force coefficient
C_L	Lift force coefficient
C_D	Drag force coefficient
C_{M_i}	Aerodynamic moment coefficient
C_{Lmin}	Minimum value of the lift force coefficient
C_{Lmax}	Maximum value of the lift force coefficient
C_{Dmin}	Minimum value of the drag force coefficient
C_{Lopt}	Optimum lift force coefficient
C_{Dopt}	Optimum drag force coefficient
FDM	Fused Deposition Modeling
i	Index corresponding to the spatial components x , y , and z , respectively
K	Lift-to-drag ratio
K_{max}	Maximum value of the lift-to-drag ratio
K_{min}	Minimum value of the lift-to-drag ratio
M_i	Aerodynamic moment component [N m]
P_i	Aerodynamic force component [N]
PIV	Particle Image Velocimetry
R	Radius of the main rotor [m]
RANS	Reynolds-Averaged Navier-Stokes
RSM	Response Surface Methodology
v	Air velocity [m/s]

Y^+	Dimensionless wall distance
α	Angles of attack [°]
β	Sideslip angle [°]
δ	Derivation
ρ	Air density [kg/m ³]

I. Introduction

Gyrocopter manufacturers offer a low level of technical advancement of classical rotorcrafts in the face of modern engineering capabilities and observed development trends. Currently, there are works in the world aimed at making propulsion systems more efficient and, in the case of gyrocopters, obtaining shortened or even vertical take-off. For example, at the Institute of Aviation in Warsaw, a team collaborating with Aviation Artur Trendak within a consortium for a project on a modern auto-rotating rotor worked on the II-28 gyrocopter head enabling vertical take-off. The method of take-off with such a head is based on changing the angle of attack of rotor blades (similar to helicopters). A rotor head of a helicopter with variable blade pitch is structurally simpler than a helicopter head, but its mass is greater than the mass of a typical helicopter head. In addition, Aviation Artur Trendak conducted R&D work on the design of innovative aircraft with a takeoff weight

of more than 560 kilograms. At the moment, gyrocopters have a lot of design limitations that reduce their operational capabilities. It is assumed that the adaptation of systems to increase dynamic stability and low-speed maneuverability in combination with the modification of the performance characteristics of the main rotor can extend the operational potential of the rotorcraft considered. An additional rotor drive in a classical gyrocopter will improve its flight characteristics and the range of its mission. The capability of vertical take-off and landing should be mentioned first as a significant impact on the current state of technology. In the future, this solution will enable operations even in urban infrastructure so such an aircraft will become more functional. A solution with an autorotating main rotor will contribute to a reduction in energy consumption, which in turn can make multicopter aircraft even more widespread. The fact that a multicopter consumes more energy during progressive flight explains the use of a light-weight, relatively uncomplicated (compared to a helicopter) auto-rotating rotor. Time of take-off, landing and hover is insignificant for total flight time and leads to a reduction in the operating time of the additional source of lift force, i.e. multiple rotors. This work presents the complete aerodynamic characteristics of the fuselage of a hybrid multi-rotor aircraft with autorotation capability, obtained by two independent methods. The former involved numerical calculation using the CFD method and the latter consisted in conducting experimental tests in a wind tunnel.

Aerodynamic forces and moments in a wind tunnel are measured using a force balance. The experiment should be initially preceded by calculations in order to choose the correct measuring range. The coefficients of aerodynamic forces and moments were calculated from the calculated or measured values of these parameters, and the obtained results were then subjected to quantitative and qualitative analysis to evaluate the developed geometry. The CFD method allows for a fast and multivariate aerodynamic analysis to achieve high accuracy of results. In this method, the fluid flow around the tested object in given boundary conditions is calculated using a defined solver. An example of this approach is presented in [1] where the impact of aerodynamic loads on the stability and control of the gyrocopter model was studied. It is also possible to study the aerodynamics of selected aircraft components [2].

Another example of the use of CFD in the aviation field is the work of [3], where electric, hybrid, and distributed propulsion systems were developed and analyzed for the four-seat DA42 Twin Star Light Aircraft to investigate their feasibility for higher performance, lower fuel consumption and emission. In the paper [4] based on CFD and rigid dynamic mesh techniques, a numerical method was developed to calculate the longitudinal and longitudinal-lateral coupling forces and moments with small amplitude sinusoidal pitch oscillation, and the corresponding dynamic derivatives of two fragment-structure-damaged and two continuous-

rod-damaged models modified from the SACCON UAV.

The developed numerical models are often validated by wind tunnel testing [5]. In the wind tunnel, it is possible to perform tests on objects used in various sectors of the economy: automotive transport [6]-[8], railroad [9], [10] or wind energy [11]-[13]. Particularly important are tests of aeronautical structures. Such tests can verify performance of these structures quickly and at a reasonably low cost before flight tests. It is possible to study both the geometry of entire scale aircraft, their components [14], and their propulsion systems. For example, the work [15] investigated the aerodynamic characteristics of a scale model gyroplane using a low-speed wind tunnel. Another example is the study by Yilmaz (2015) [16] which analyzed the performance of a ducted propeller designed for UAV applications. A study of the aerodynamic characteristics of a fully adaptive aircraft configuration using a wind tunnel was presented by Neal (2004) [17]. Wind tunnel results showed that variable planform capability enables low drag over a range of flight conditions. Nicolosi (2016) [18] presented the experimental estimation of both longitudinal- and lateral-directional aerodynamic characteristics of an aircraft. Wind tunnel tests also allow the evaluation of aerodynamic interference of the aircraft [19] or measurements of aerodynamic interference of a hybrid aircraft with multicopter propulsion [20]. Wind tunnel testing can be extended by the measurement of the flow field around the test object using, for example, Particle Image Velocimetry (PIV) [21]. Unfortunately, wind tunnels often are used long support systems of models with a low level of damping, which affects the nature of the flow around the object and the generation of turbulence during the experiments. This can also result in low-frequency, high-amplitude resonance, which leads to poor data quality and limited test range. To achieve the planned range of tests and obtain high-quality results, an active vibration control system can be used [22]. This system is based on stacked piezoelectric actuators with velocity feedback read by an accelerometer. This solution improves the stability of the support structure and the safety of testing objects in the wind tunnel. A common method to study aircraft aerodynamics is to conduct coupled analyses based on CFD models using inputs from wind tunnel tests. [23], [24] An example is [25] where the results from wind tunnel testing were applied to create a high-fidelity aerodynamic model of the tandem tilt wing, distributed electric propulsion, vertical takeoff and landing aircraft. In other example, an accurate flutter prediction method based on computational fluid dynamics was proposed to determine the flutter dynamic pressure of a wind tunnel model before flutter test [26]. The paper [27] reviews how CFD simulations have been used for predicting separated flows, and the associated aerodynamic performance, throughout the flight envelope, giving special focus to NATO aircraft. Shah (2002) [28] studied low-speed static and dynamic wind tunnel tests of a commercial transport configuration over an extended angle of

attack/sideslip envelope. The results obtained enable simulations for determining aircraft flight characteristics in extreme and loss-of-control conditions. Wind tunnel tests can also be coupled with flight test data to analyze aerodynamic parameters by mathematical modeling [29].

A collection of test data from several aircraft models can be used to develop a generic global aerodynamic model for aircraft [30]-[32]. Statistical methods such as RSM (Response Surface Methodology) can also be used in wind tunnel testing to evaluate the aerodynamic behavior of the aircraft [33]. The aerodynamic characteristics of aircraft can also be modelled mathematically [34], [35]. The basic characteristics obtained in a numerical way allow investigation of the gyroplane longitudinal static stability for the selected stabilizer angles [36]. The idea presented in this paper is based on combining the advantages of a gyrocopter (as an aircraft with a light and simple structure, cheap to operate) with a multirotor system allowing for a shorter take-off or vertical take-off and landing. This, in turn, provides stable and safer low-speed flight. The combination of these two types of aircraft results in an innovative means of individual air transport. The article analyses a novelty design of an aircraft with a new type of stabilizer whose shapes, mainly conventional and inverted V-tail, have been used so far in aviation. The stabilizer was designed by the authors of this paper. The proposed X-tail solution is a variation of both of these types of tail in a single boom arrangement. This approach represents a new, original concept of stabilizer geometry the authors also investigated in a simulation.

The remainder of this paper is structured as follows.

Section II describes the research object which is a unique construction combining an autogyro and a multicopter. Section III presents the research methodology based on numerical analysis and wind tunnel experiments. Section IV presents the data processing and discusses the obtained aerodynamic coefficients and lift to drag curves. The last section summarizes the conducted research.

II. Research Object

The object of this study was a hybrid aircraft which is a combination of a gyrocopter and a multicopter (Figure 1). Detailed theoretical aspects related to gyrocopter aerodynamics are presented in [37]. The aircraft is being built within the LIDER X project funded by the Polish National Centre for Research and Development. The concept assumes the use of an auto-rotating main rotor to perform basic flight. Four additional rotors placed in pairs at the front and rear enable vertical take-off, landing, and hovering. Forward flight will be performed thanks to the pull force generated by the rear engines capable of axial rotation.

The proposed dual propulsion system concept provides safer and stable low-speed flight. Figure 2 shows the selected versions of the designed unmanned aerial vehicle.



Fig. 1. Visualization of the designed aircraft



Fig. 2. View of selected versions of the designed unmanned aerial vehicle

The second version of the developed geometry was analyzed in this paper. The third version is optimized and is in line with the comments and suggestions discussed in the article. The aerodynamic properties of the fuselage and tail (stabilizer) were investigated for the model without a propulsion system (propellers and engines).

The aim of this research was to determine aerodynamic characteristics of the model for different angles of attack α and sideslip angles β . The geometry of the model consists of three main parts. The first one is a fuselage with a mast. In the rear part, the fuselage passes into a tail and an X-type stabilizer with installed tail rotors and a landing gear. Arms with front rotors are mounted at the front of the aircraft. The geometric dimensions of the model are $916 \times 583 \times 440$ mm (length \times width \times height). An auto-rotating rotor in a gyrocopter is driven by downward airflow so it is considered that the operation of the auto-rotating rotor does not significantly affect the forces acting on the fuselage and stabilizer parts. Besides, the main rotor for this object measures 1.8 m, and it is difficult to perform wind tunnel tests at a scale of 1:1. To validate the numerical model, a test object configuration with the fuselage and the stabilizer was investigated. The main rotor is the object of the further research because the fuselage with the stabilizer should provide stability. If this is the case, then in autorotation flight, the relationship between the lift force of the main rotor and the thrust force of the push/pull propeller is very important. The main rotor in this type of aircraft is, therefore, often tested separately.

III. Methodology

III.1. CFD Method

Mathematical description for all theoretical fluid

dynamics models is based on the Navier-Stokes equations which describe the motion of viscous fluid domains. Studies on fluids follow equations which are based on the law of conservation of physical properties of the fluid. The basic equations are three laws: the equation of conservation of mass, the equation of conservation of momentum, and the equation of conservation of energy. RANS-based numerical calculations were performed in the Ansys Fluent software. The developed aircraft geometry was imported into the Design Modeler module. A rectangular computational domain was created with wall offset by 2 m on each side in y - and z - directions and 3 m in the x -direction, i.e. in front of and behind the fuselage. The model was divided into several sections, and the aerodynamic forces and moments were calculated relative to the adopted coordinate system, as shown in Figure 3. In the Mesh module, a computational mesh of 3 597 410 elements was created. Edge Sizing and Face Sizing functions were used to improve the quality of the created mesh. Inflation was used to create a boundary layer around the surface of the test object. The generated computational mesh visible on the outer surface of the research object is shown in Figure 4. The number of mesh elements and their size were selected so that further enlargement of the grid generates differences in results not exceeding 1%. For the entire research object, the value of Y^+ is in the range from 0.5994 to 47.2022.

Considering the stabilizer itself, the maximum value is reduced to 29.6229, whereas the maximum value on the front arms is 33.7831 so the use of wall functions is justified. The $k-\omega$ SST model was selected as a turbulence model because it enables a faster convergence and better results than the $k-\varepsilon$ one. The $k-\varepsilon$ model was applied for the outer region and outside the boundary layer and the $k-\omega$ one for the internal boundary layer.

The turbulence intensity defined in the model was 1% and the turbulence length scale was 0.28 m.

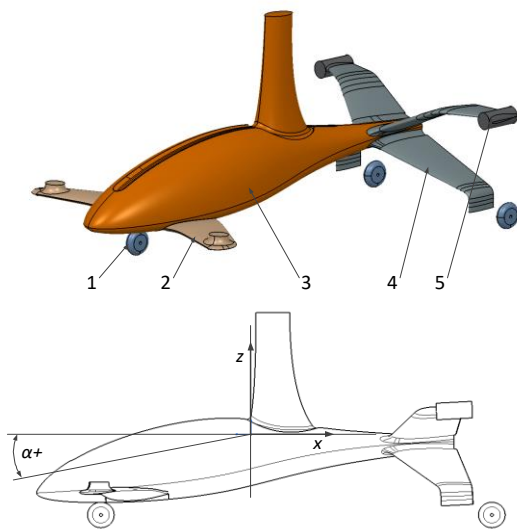


Fig. 3. Geometric model of the designed aircraft with the assumed coordinate system and direction of the angle of attack, 1. wheels, 2. arms, 3. fuselage with mast, 4. stabilizer, 5. nacelle

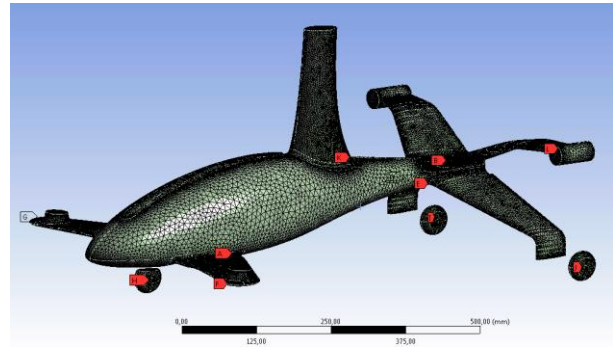


Fig. 4. Computational mesh on the outer surface of the research object

The geometric model created was placed in the geometric center of the cuboidal computational domain.

Its dimensions are $6916 \times 4582 \times 4439$ mm (length \times width \times height) (Figure 5). An velocity inlet type was created on one surface of the domain, while an pressure outlet type was defined on the opposite surface. The remaining walls of the domain were defined as wall. A working gas was assumed to be air defined as ideal gas.

Air flow velocity was set to 20 m/s. Air density corresponded to normal conditions, i.e. temperature of 15 °C and pressure of 1013.25 hPa. Its dynamic viscosity was set to $17.894 \mu\text{Pa s}$. The tests were conducted for a set of measurement points defined by the angle of attack ranging from -20 to $+20$ degrees.

III.2. Wind Tunnel

The experimental tests were conducted in a closed-circuit subsonic wind tunnel located in the aerodynamics laboratory at the Center for Innovation and Advanced Technology at the Lublin University of Technology.

Figure 6 shows a general view of the wind tunnel where the tests were conducted, and Table I lists main sensors used in the wind tunnel. In addition, a barometric pressure transducer DeltaOHM HD 9408T BARO was used in the wind tunnel. The model for the real-scale wind tunnel tests was made in 3D printing using the FDM method. The test object was placed in a 1275×1415 mm measurement chamber on a six-component balance FMT 625-1b manufactured by the Maritime Advanced Research Centre (Figure 8).

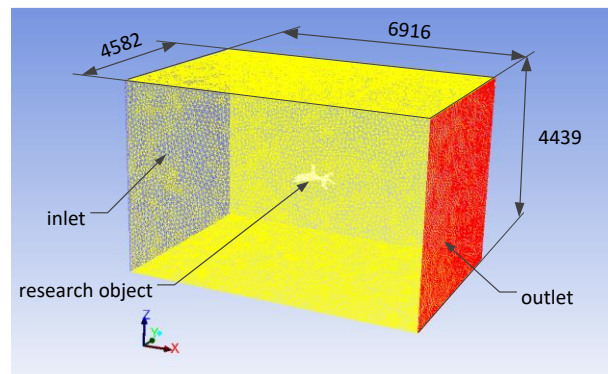


Fig. 5. Computational domain with the research object

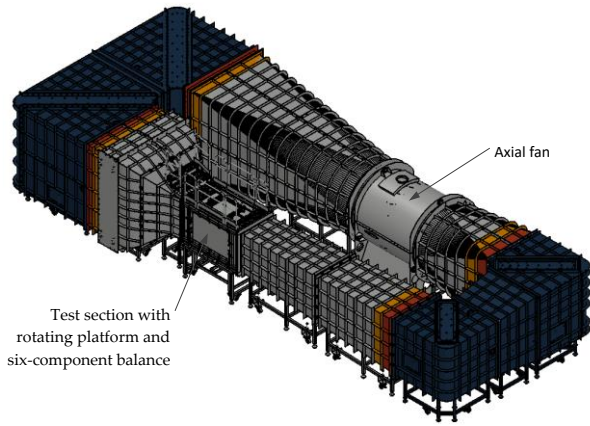


Fig. 6. General view of the wind tunnel

TABLE I
LIST OF MAIN SENSORS USED IN THE WIND TUNNEL

Measurement point symbols	Measured parameters	Type of equipment	Measured value range
DP1, DP2	Pressure difference	Differential pressure transducer	0-2.5 kPa
TH1, TH2, T1, T2	Temperature	Aplisens APR-2000G	-20-80°C
RH1, RH2, RH	Humidity	Humidity sensor with temperature measurement	0-100% RH
U1	Velocity (cooler)	ASCE HD4917T	0-15 m/s
U2, U3	Velocity (measuring chamber)	Humidity sensor with temperature measurement	0-70 m/s

The balance works with the measuring amplifier MX840B HBM. The external diameter of the balance is 25 mm. On the rotating platform (TWOS 3030-E), the balance is mounted on a conical connection and an M25x1.5 threaded bottle screw (left-hand thread in the dynamometer).

A feather key is used to ensure angular alignment. The balance tip the model is attached to has a diameter of 16 mm - the angular positioning of the model is achieved using a feather key. The model is screwed to the balance with an M5 grub screw. In the front of the measuring tip, the model is screwed to the transmitter with an M5 grub screw. In the front of the measuring tip, there is an additional M6 threaded hole that can be used to attach or remove the tested model. Figure 7 indicates the location of the sensors used in the wind tunnel. Their description is given in Table I.

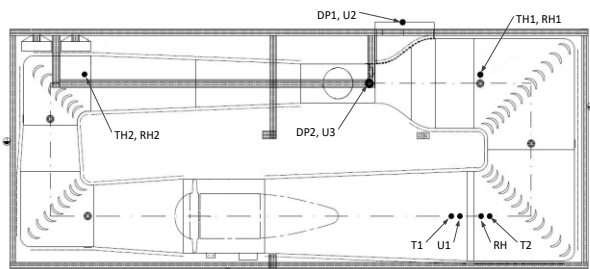


Fig. 7. Arrangement of the main sensors used in the wind tunnel (symbols as in Table I)

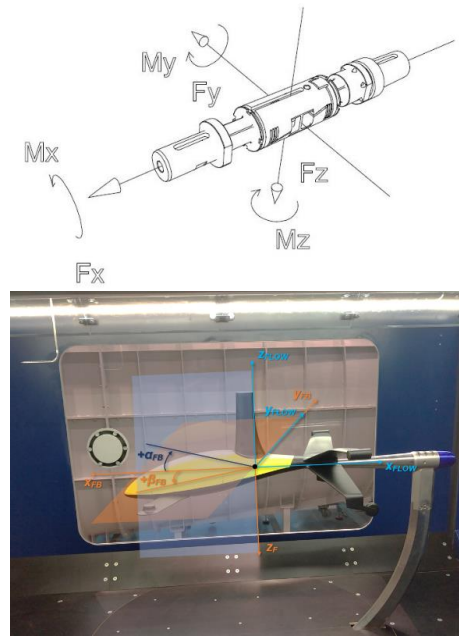


Fig. 8. Coordinate system of the FMT625-1b force balance adopted flow-related reference system

The wind tunnel fan allows for a maximum flow velocity in the chamber of 60 m/s at a turbulence intensity of less than 0.3%. The balance used enabled us to measure the three components of aerodynamic force and moment in the balance coordinate system. The coordinate system was then transformed to the flow coordinate system. The balance is a monolithic instrumented transducer using a set of strain gages. The measurement ranges and average error for each of the components measured by the balance are shown in Table II. The balance was installed on a sting inside the measurement chamber. The rotating platform and mast allowed adjustment of the angle of attack and the sideslip angle. The tested aircraft model is depicted in Figure 9.

The model was put on the scale from the rear side of the aircraft. Other types of supporting systems and their interference on aerodynamic characteristics of an aircraft model in a low-speed wind tunnel are presented in [38].

Similar to the numerical calculation, the angle of attack was changed from 20 to +20 degrees, in 5-degree increments. The sideslip angle was adjusted from -20 to 0 degrees, in 5-degree increments. The airflow velocity was measured using a Prandtl tube with a measurement range of 3÷100 m/s, and its value was adjusted by changing the setting on the inverter of the electric motor driving the axial fan.

TABLE II
MEASURING RANGE AND AVERAGE ERROR
OF THE MEASURED VALUES

Component	Range	Average error
F_x	-207 ÷ +206 N	0.11%
F_y	-241 ÷ 251 N	0.15%
F_z	-620 ÷ +620 N	0.08%
M_x	-37.7 ÷ +38.2 Nm	0.04%
M_y	-27.4 ÷ +27.4 Nm	0.07%
M_z	-21.4 ÷ +21.4 Nm	0.07%



Fig. 9. Research object during the wind tunnel testing

The measured pressure value was converted by the Aplisens APR 2000G transmitter. The velocity values for which the measurements were performed varied in the range of 5-20 m/s, in 5 m/s increments. Due to a large number of obtained results, it was decided to present here the results for a velocity of 20 m/s which corresponds to the assumed cruising velocity. The HBM MX840B measuring amplifier was used to acquire the measurement signals. For each position and air velocity, forces and moments were measured for 5 seconds at a sampling rate of 25 Hz. The obtained values were averaged. The process of parameter adjustment and data acquisition was controlled from a computer.

Additionally, the atmospheric conditions inside the measurement chamber were measured. The average air temperature was equal to 18.5 °C and air humidity was 21%.

IV. Results Analysis

IV.1. CFD Method

The values of three components of aerodynamic force and moment were obtained from the numerical calculations. These were drag force, lift force, side force, roll moment, pitch moment and yaw moment, respectively. From the obtained values, the corresponding aerodynamic coefficients were calculated according to equations (1) and (2):

$$C_i = \frac{P_i}{0.5\rho v^2 \pi R^2} \quad (1)$$

$$C_{Mi} = \frac{P_i}{0.5\rho v^2 \pi R^3} \quad (2)$$

where C_i is the aerodynamic force coefficient, C_{Mi} is the aerodynamic moment coefficient, M_i is the aerodynamic moment component (N m), P_i is the aerodynamic force component (N), i is the index corresponding to the spatial components x , y , and z , respectively, R is the radius of the main rotor, which is 0.9 m, ρ is the air density of 1.2255 kg/m³ corresponding to a temperature of 288.15

K, v is the air velocity as 20 m/s. Figure 10 shows the drag force coefficient C_D and the lateral force coefficient C_{SF} as a function of the angle of attack α . The minimum value of drag force coefficient equal to 0.0053 was obtained for angle $\alpha = 5^\circ$.

The additional arms added to the fuselage account for from 15% ($\alpha = 0^\circ$) to 29% ($\alpha = 20^\circ$) of the total drag force. The fuselage and mast contribute between 22% and 44% of the generated drag force. In the case of C_{SF} , due to the zero-sideslip angle, small deviations from 0 were obtained (an order of magnitude smaller than in the case of C_D), which is due to calculation errors (resulting, for example, from the asymmetry of the calculation mesh and the adopted sectioning of the geometry). Figure 11 shows the lift coefficient C_L and roll moment coefficient C_{Mx} as a function of the angle of attack α . The main contribution to lift is from the stabilizer which generates 44% of the total lift for angle $\alpha = -20^\circ$ and 47% for $\alpha = 20^\circ$. The lift force is zero for $\alpha = 3.5^\circ$.

Figure 12 shows the pitch moment coefficient C_{My} and yaw moment coefficient C_{Mz} as a function of the angle of attack α . In the considered case, the main influence on the pitch moment is exerted by the stabilizer, however, the fuselage with the mast and the arms in the front part of the fuselage generates the opposite moment. For the given range of extreme angles of attack, e.g. $\alpha = -20^\circ$, the moment generated from the fuselage and the mast (together) is 36% in relation to the stabilizer, and for the arms, this value reaches up to 66%, which in total gives a value higher by 102% in relation to the stabilizer.

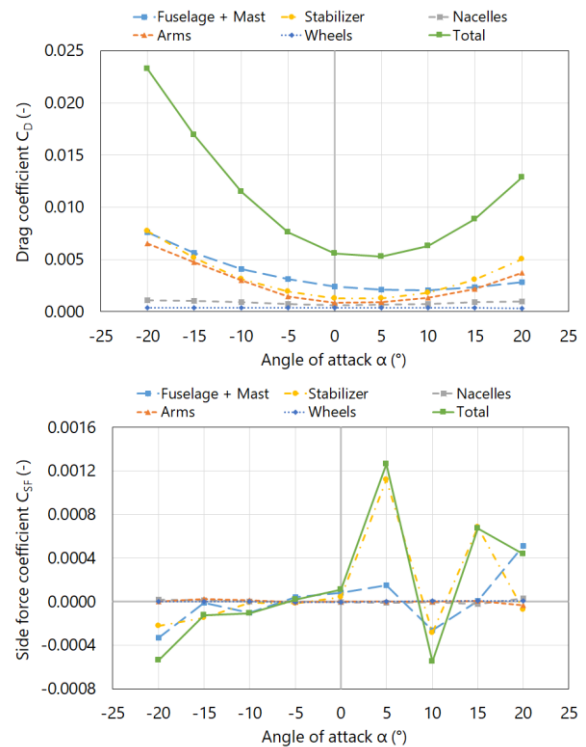


Fig. 10. Drag coefficient (top) and side force coefficient (bottom) for the analyzed angles of attack and angles of sideslip for the airflow velocity equals 20 m/s

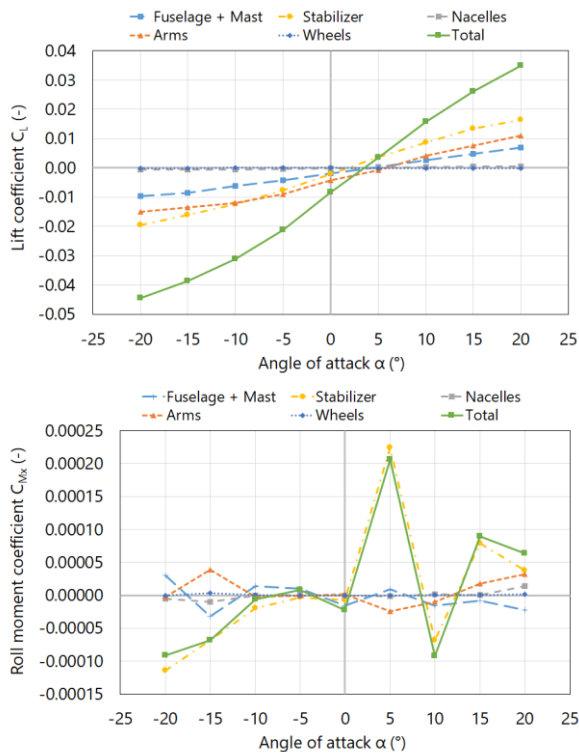


Fig. 11. Lift coefficient (top) and roll moment coefficient (bottom) for the analyzed angles of attack and angles of sideslip for the airflow velocity equals 20 m/s

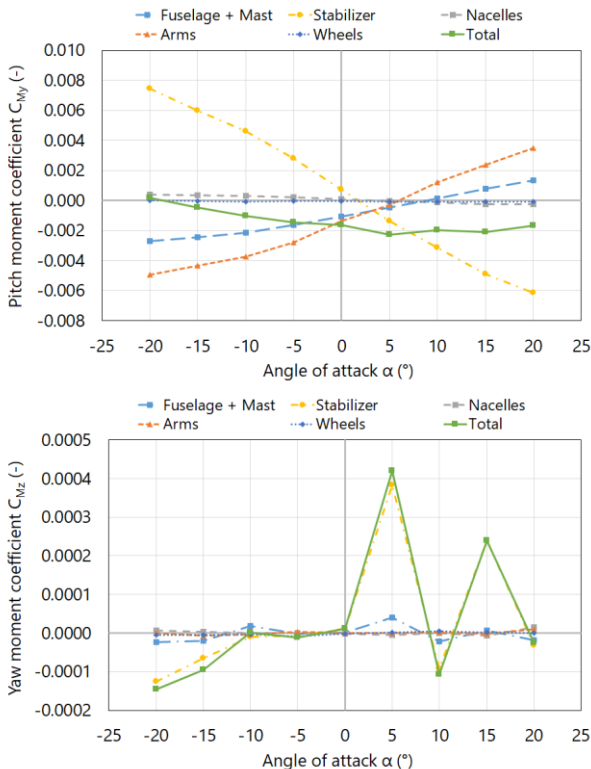


Fig. 12. Pitch moment coefficient (top) and yaw moment coefficient (bottom) for the analyzed angles of attack and angles of sideslip for the airflow velocity equals 20 m/s

This difference increases to 113%, 128%, and 160%, respectively. Even larger values are obtained for the

small angles of attack (around $\alpha = 0^\circ$) due to the relatively small absolute values of the pitch moment obtained. For the positive angles of attack, these values reach 79% ($\alpha = 20^\circ$). Analysis of the obtained values confirms that the arms interact strongly with the aircraft worsening its aerodynamic characteristics. This is because the characteristics of the pitch moment were obtained, which is a decreasing function only in a certain range. This has a direct effect on the stability of the tested object. By eliminating the arms from the structure, the correct character of the pitch moment is obtained.

Then, in the whole range of the angle of attack, the function is decreasing and its derivative in function α is less than 0. In the case of C_{Mz} , due to the zero sideslip angle, small deviations from 0 were obtained (by the order of magnitude smaller than in the case of C_{My}), which is caused by calculation errors. Figure 13 shows the drag curve for the tested fuselage. Its shape is similar to a parabola with a horizontal axis of symmetry. It is one of the universal aerodynamic characteristics to determine characteristic aerodynamic parameters of the tested aircraft model, e.g. C_{Lmin} , C_{Lmax} , C_{Dmin} , C_{Lopt} , C_{Dopt} .

These values are -0.0445, 0.0349, 0.0053, 0.0260, and 0.0087, respectively. For small values of the angle of attack, the drag constitutes several percent of the total drag. In the range of linear variation of the lift coefficient with the angle of attack, the drag coefficient increases approximately with the quadratic of the lift coefficient, and outside this range, it increases much faster. In addition, Figure 13 shows the lift-to-drag ratio K as a function of the angle of attack α .

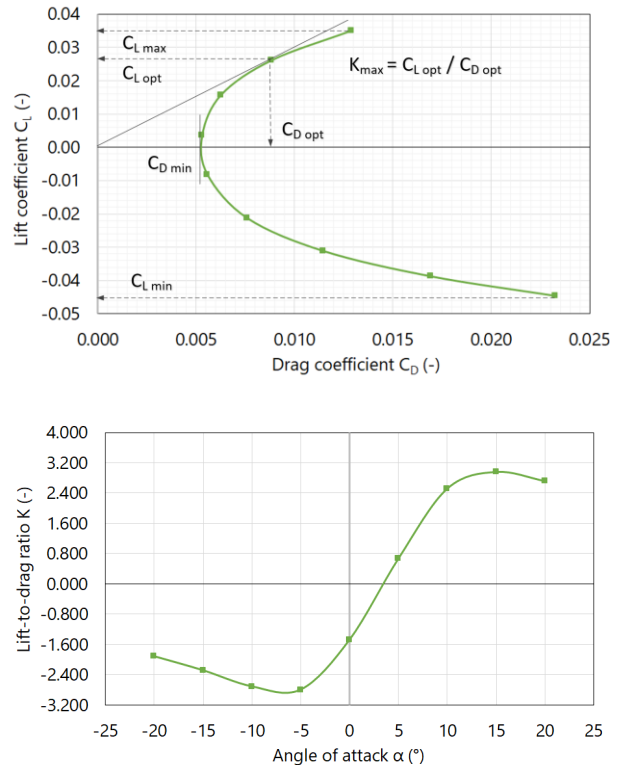


Fig. 13. Drag curves for the research object for the airflow velocity equals 20 m/s and lift-to-drag ratio as a function of the angle of attack

The extreme values of this ratio for the investigated fuselage model occur for the angle of attack $\alpha = -5^\circ$ for $K_{\min} = -2.8$ and at the angle $\alpha = 15^\circ$ for $K_{\max} = 3.0$, while $K = 0$ is obtained at the angle of attack $\alpha = 3.5^\circ$ for $C_L = 0$.

IV.2. Wind Tunnel

As in the case of numerical calculations, the aerodynamic characteristics of the tested model were created from the results of the wind tunnel tests. The first parameter considered is the drag force coefficient as a function of the angle of attack for the defined sideslip angles (Figure 14). The drag coefficient varied in the range from 0.005 to 0.024, with the smallest value for the zero angle of attack and the largest values for the extreme angles of attack. An increase in the value of the angle (both positive and negative) resulted in an increase in the value of the drag coefficient. The drag also increased as the sideslip angle increased. For the zero angle of attack, it increased from 0.005 to 0.008 for a sideslip angle of 20° .

The second part of Figure 14 shows the side force coefficient. For the zero sideslip angle, its value was approximately zero over the entire range of the angle of attack considered. The small non-zero value was due to the non-ideal symmetry of the aircraft model. Moreover, in the range of low forces, the force balance had a larger measurement error, which resulted in a non-zero value of the measured force.

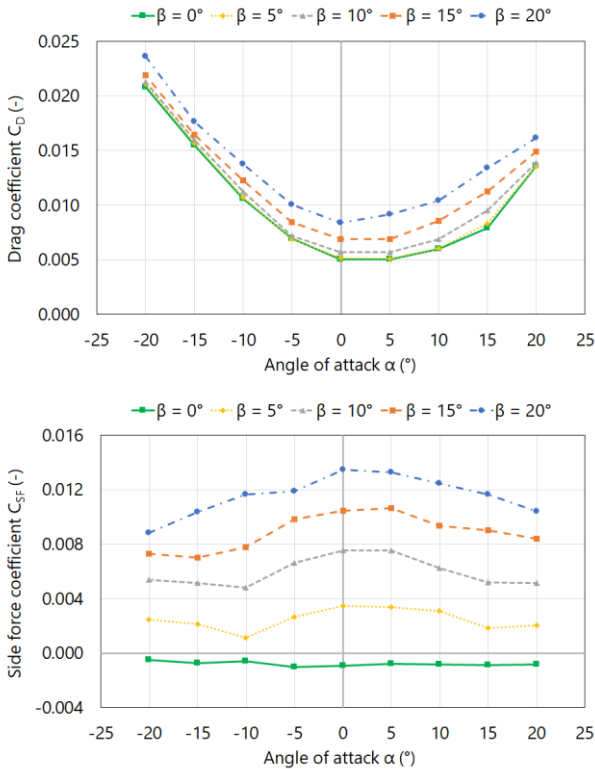


Fig. 14. Drag coefficient (top) and side force coefficient (bottom) for the analyzed angles of attack and angles of sideslip for the airflow velocity equals 20 m/s

The next parameter analyzed was the lift coefficient (Figure 15). It can be observed when the value of the coefficient increases with the increasing angle of attack in the entire analyzed range. For the considered sideslip angles, the differences were insignificant. For larger sideslip angles, the coefficient took smaller values for large attack angles (positive and negative). For the zero angle of attack, the lift force was close to zero. The coefficient varied from -0.032 to 0.032. Next, the coefficients of aerodynamic moments were analyzed.

The first of them was the roll moment coefficient (Figure 15). The value of this coefficient varied from -0.0005 to 0.0009 and was approximately equal to zero for the zero angle of attack. This is because the model is symmetrical and the aircraft is balanced along the longitudinal axis. An increase in the sideslip angle results in an increase in the absolute value of the moment. The observed differences increase as the angle of attack increases.

The pitch moment coefficient (Figure 16) plays an important role in the assessment of the aerodynamic properties of the tested aircraft. Its value is strictly related to longitudinal stability. The calculated value of the pitch moment coefficient varied from -0.0028 to -0.0003. For all considered sideslip angles pitch moment had a decreasing trend in the range of the angles of attack from -25 to -5 degrees. Above this angle value, the trend became increasing. The lack of a continuously decreasing trend indicates a stability problem in the range of positive angles of attack.

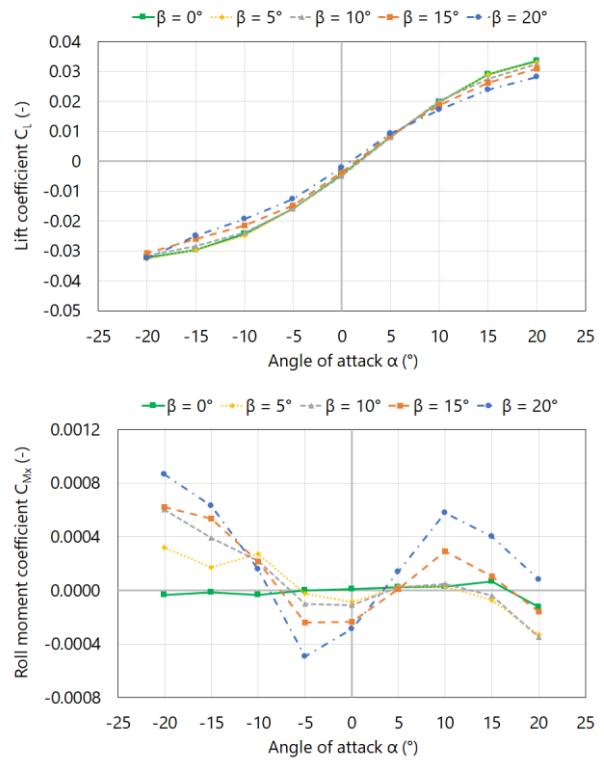


Fig. 15. Lift coefficient (top) and roll moment coefficient (bottom) for the analyzed angles of attack and angles of sideslip for the airflow velocity equals 20 m/s

In addition, the moment coefficient is negative over the entire range of angles of attack. For a structure with correct longitudinal stability, the derivative of the function describing the pitch moment M_y reaches negative values (Eq. (3)). Static longitudinal stability was examined according to this stability criterion:

$$\frac{\delta M_y}{\delta \alpha} < 0 \quad (3)$$

The last coefficient considered is the yaw moment coefficient (Figure 16). Its value varied from 0 to 0.0016.

As in the case of roll moment for the zero angle of attack, the value of the yaw moment coefficient was approximately equal to zero because of the symmetry of the tested model. As the sideslip angle increased, the coefficient value gradually increased. The largest values occurred for the zero angle of attack. The exceptions are the largest sideslip angles, i.e. 15 and 20 degrees for which the extreme values shifted toward larger angles of attack. Figure 17 shows the drag curve for the tested fuselage obtained from the wind tunnel tests for β ranging from 0° to 20° , in 5° increments. The values of aerodynamic parameters of the tested aircraft model for $\beta = 0^\circ$ are $C_{Lmin} = -0.0323$, $C_{Lmax} = 0.0336$, $C_{Dmin} = 0.0050$, $C_{Lopt} = 0.0270$, and $C_{Dopt} = 0.0070$, respectively.

Moreover, Figure 18 shows the lift-to-drag ratio K as a function of the angle of attack α for the considered sideslip angles.

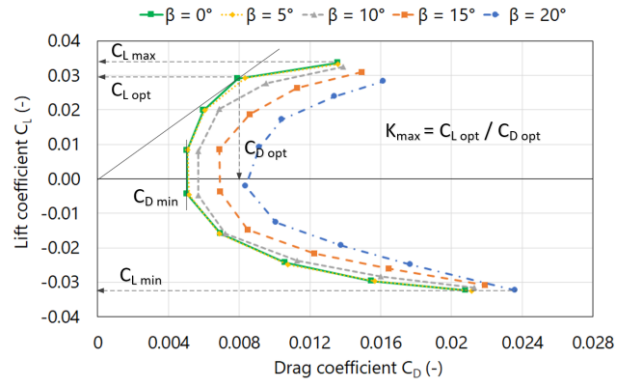


Fig. 17. Drag curves for the research object for the airflow velocity of 20 m/s

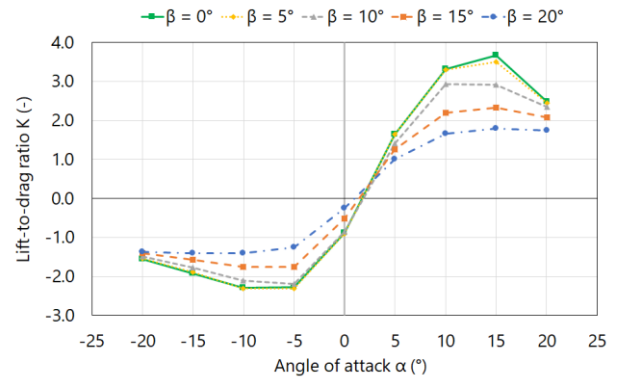


Fig. 18. Lift-to-drag ratio as a function of the angle of attack

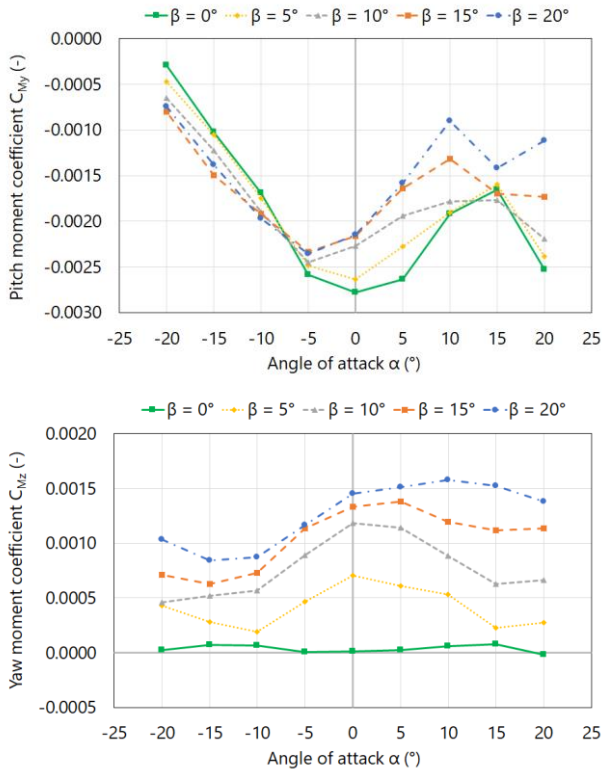


Fig. 16. Pitch moment coefficient (top) and yaw moment coefficient (bottom) for the analyzed angles of attack and angles of sideslip for the airflow velocity equals 20 m/s

The extreme values of this ratio for the investigated fuselage model occur for the angle of attack $\alpha = -10^\circ$ for $K_{min} = -2.3$, and for the angle $\alpha = 15^\circ$ for $K_{max} = 3.7$, while $K = 0$ was obtained for the angle of attack $\alpha = 1.75^\circ$ for $C_L = 0$.

IV.3. Comparison of Wind Tunnel and CFD Analysis Results

Figures 19-21 compare the aerodynamic characteristics for the wind tunnel and CFD analysis for the angles of attack at the airflow velocity of 20 m/s. Due to the symmetrical flow, it was decided to present the drag coefficient, lift coefficient and pitch moment coefficient.

As shown in these figures, the characteristics are similar for both the drag coefficient and the lift coefficient. The largest differences occur for the negative values of the angle of attack and do not exceed 0.002 for the drag coefficient and 0.01 for the lift coefficient.

The characteristics of the pitch moment coefficient C_{M_y} show similar trends in the range of negative angles of attack (decreasing functions). For the positive values of the angle of attack for both methods, a problem with the longitudinal stability of the research object was observed. The largest differences in the values of the pitch moment coefficient were observed close to the angle of attack $\alpha=0$.

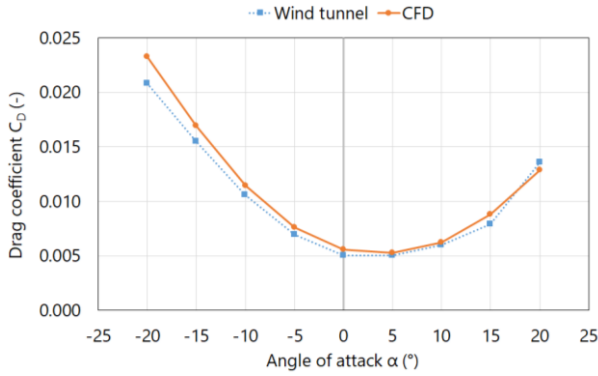


Fig. 19. Comparison of the drag coefficient for the wind tunnel and CFD analysis for the analyzed angles of attack and angles

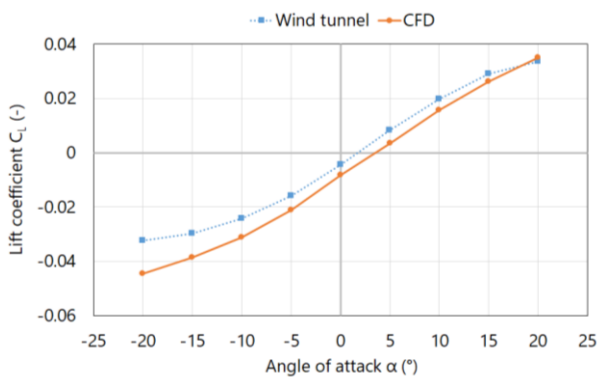


Fig. 20. Comparison of the lift coefficient for the wind tunnel and CFD analysis for the analyzed angles of attack

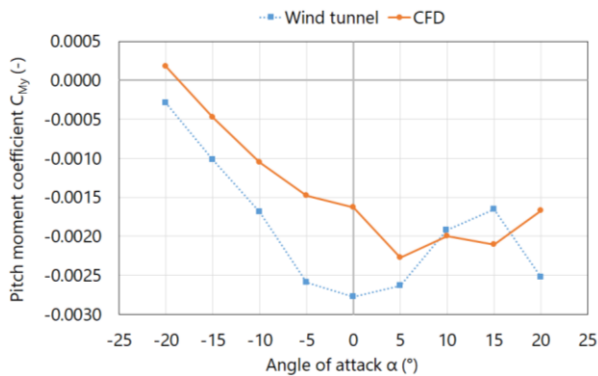


Fig. 21. Comparison of the pitch moment coefficient for the wind tunnel and CFD analysis for the analyzed angles of attack

V. Conclusion

This paper analyzes the results of the fuselage aerodynamics of a hybrid unmanned aerial vehicle. The CFD numerical analysis was performed in the first part of the study, and the second part presents the results of wind tunnel tests. In both cases, aerodynamic forces and moment were obtained as a function of the angle of attack for a defined set of sideslip angles. The obtained values were converted into corresponding aerodynamic coefficients. The obtained results allowed us to develop characteristics of aerodynamic forces and moments.

Their analysis enabled us to evaluate the most

important aerodynamic properties of the designed aircraft, to assess its stability, and to modify it in terms of optimization. The obtained values of drag and lift force coefficients indicate favorable aerodynamic properties of the studied geometry. However, due to the significant size of the arms at the front of the fuselage, the longitudinal stability significantly deteriorated over the entire range of angles of attack. There was a problem with the longitudinal stability of the considered fuselage geometry including the stabilizer. The derivative of the function describing the pitch moment coefficient C_{My} as a function of the angle of attack α does not reach negative values in the whole range of the considered angle of attack. The pitch moment generated by the stabilizer is described by a decreasing function in the whole range of the angle of attack. Unfortunately, the fuselage with the mast and the arms mounted in the front part generate definitely too large a counter-moment which has a negative influence on the aircraft stability. Considering the obtained results, it was decided to introduce further geometry modifications aiming at decreasing the drag force, and the pitch moment generated by the arms. This will be achieved by decreasing the cross-sectional area of the arms mounted in the front part of the fuselage and increasing the distance of the stabilizer from the assumed center of the coordinate system. The numerical studies resulted in many modifications to optimize the design.

The performed wind tunnel tests confirmed the satisfactory correlation of the simulation results with the experiment. Comparing the developed aerodynamic characteristics for the CFD model and the model from the wind tunnel tests, it can be observed that the results obtained for the drag coefficient, lift coefficient and drag curve are very comparable. Similar results were also obtained for the pitch moment coefficient. The curves for roll and yaw moment coefficients show greater differences due to very small absolute values of the obtained moments, which translates into much larger error in their calculation or measurement. In further work, it is planned to include correction values in the created numerical model to make computational and experimental results more comparable.

Acknowledgements

This work has been financed by the Polish National Centre for Research and Development under the LIDER program Grant Agreement No. LIDER/27/0140/L-10/18/NCBR/2019.

References

- [1] T. Lusiak, A. Novak, M. Bugaj, R. Madlenak, Assessment of Impact of Aerodynamic Loads on the Stability and Control of the Gyrocopter Model, *Communications-Scientific letters of the University of Zilina*. 2020, 22(4), 63-69.
- [2] K. Szwedziak, T. Lusiak, Z. Grzywacz, K. Drozd, Numerical CFD Analysis of an Aerodynamic Head Cover of a Rotorcraft Motor, *Communications-Scientific letters of the University of Zilina*. 2018, 20(3), 42-47.
- [3] G. M. Bravo, N. Praliyev, N., A. Veress, Performance analysis of

- hybrid electric and distributed propulsion system applied on a light aircraft, *Energy*. 2021, 214, 118823.
- [4] B.G. Mi, Simulation on the dynamic stability derivatives of battle-structure-damaged aircrafts, *Defence Technology*. 2021, 17(3), 987-1001.
- [5] D. Favier, The role of wind tunnel experiments in CFD validation, *Encyclopedia of Aerospace Engineering*, John Wiley & Sons, 2010.
- [6] F. Cheli, R. Corradi, D. Rocchi, G. Tomasini, E. Maestrini, Wind tunnel tests on train scale models to investigate the effect of infrastructure scenario, *Journal of Wind Engineering and Industrial Aerodynamics*. 2010, 98(6-7), 353-362.
- [7] A. Cogotti, F. De Gregorio, Presentation of flow field investigation by PIV on a full-scale car in the Pininfarina wind tunnel, *SAE transactions*. 2000, 1417-1442.
- [8] C. Bayındır, Y. E. Akansu, M. Salman, The determination of aerodynamic drag coefficient of truck and trailer model by wind tunnel tests, *International Journal of Automotive Engineering and Technologies*. 2016, 5(2), 53-60.
- [9] L. D. Zhu, L. Li, Y. L. Xu, Q. Zhu, Wind tunnel investigations of aerodynamic coefficients of road vehicles on bridge deck, *Journal of fluids and structures*. 2012, 30, 35-50.
- [10] J. R. Bell, D. Burton, M. Thompson, A. Herbst, J. Sheridan, Wind tunnel analysis of the slipstream and wake of a high-speed train, *Journal of Wind Engineering and Industrial Aerodynamics*. 2014, 134, 122-138.
- [11] K. N. Morshed, M. Rahman, G. Molina, M. Ahmed, Wind tunnel testing and numerical simulation on aerodynamic performance of a three-bladed Savonius wind turbine, *International Journal of Energy and Environmental Engineering*. 2013, 4(1), 1-14.
- [12] M. S. Selig, B. D. McGranahan, Wind tunnel aerodynamic tests of six airfoils for use on small wind turbines, *Journal of Solar Energy Engineering*. 2004, 126(4), 986-1001.
- [13] C. L. Bottasso, F. Campagnolo, V. Petrović, Wind tunnel testing of scaled wind turbine models: Beyond aerodynamics, *Journal of Wind Engineering and Industrial Aerodynamics*. 2014, 127, 11-28.
- [14] R. Mustak, M. H. O. R. Molla, M. Mashud, Improvement of Aerodynamic Characteristics of an Airfoil by Surface Modification, *American Journal of Engineering Research (AJER)*. 2017, 6(3), 07-14.
- [15] F. N. Coton, L. Smrcek, Z. Patek, Aerodynamic characteristics of a gyroplane configuration, *Journal of Aircraft*. 1998, 35(2), 274-279.
- [16] E. Yilmaz, J. Hu, CFD Study of Quadcopter Aerodynamics at Static Thrust Conditions. In *Proceedings of the ASEE Northeast 2018 Annual Conference*, West Hartford, CT, USA, 27-28, 2018.
- [17] D. Neal, M. Good, C. Johnston, H. Robertshaw, W. Mason, D. Inman, Design and wind-tunnel analysis of a fully adaptive aircraft configuration. In *Proceedings of the 45th AIAA/ASME/ASCE/AHS/ASC Structures, Structural Dynamics & Materials Conference*, p. 1727, 2004.
- [18] F. Nicolosi, S. Corcione, P. Della Vecchia, Commuter aircraft aerodynamic characteristics through wind tunnel tests, *Aircraft Engineering and Aerospace Technology*. 2016, 88(4), 523-534.
- [19] K. Chen, Z. Shi, S. Tong, Y. Dong, J. Chen, Aerodynamic interference test of quad tilt rotor aircraft in wind tunnel, *Proceedings of the Institution of Mechanical Engineers, Part G: Journal of Aerospace Engineering*. 2019, 233(15), 5553-5566.
- [20] Z. Czyż, M. Wendeker, Measurements of Aerodynamic Interference of a Hybrid Aircraft with Multicopter Propulsion, *Sensors*. 2020, 20(12), 3360.
- [21] Z. Czyż, P. Karpiński, W. Stryczniewicz, Measurement of the Flow Field Generated by Multicopter Propellers, *Sensors*. 2020, 20(19), 5537.
- [22] W. Liu, M. Zhou, Z. Wen, Z. Yao, Y. Liu, S. Wang, X. Cui, X. Li, B. Liang, Z. Jia, An active damping vibration control system for wind tunnel models, *Chinese Journal of Aeronautics*. 2019, 32(9), 2109-2120.
- [23] U. Cella, M. E. Biancolini, Aeroelastic analysis of aircraft wind-tunnel model coupling structural and fluid dynamic codes, *Journal of Aircraft*. 2012, 49(2), 407-414.
- [24] O. J. Boelens, CFD analysis of the flow around the X-31 aircraft at high angle of attack, *Aerospace Science and Technology*. 2012, 20(1), 38-51.
- [25] B. M. Simmons, P. C. Murphy, Wind Tunnel-Based Aerodynamic Model Identification for a Tilt-Wing, Distributed Electric Propulsion Aircraft. In *Proceedings of the AIAA SciTech 2021 Forum*, p. 1298, 2021.
- [26] T. Guo, D. Lu, Z. Lu, D. Zhou, B. Lyu, J. Wu, CFD/CSD-based flutter prediction method for experimental models in a transonic wind tunnel with porous wall, *Chinese Journal of Aeronautics*. 2020, 33(12), 3100-3111.
- [27] A. Rizzi, J. M. Luckring, Historical development and use of CFD for separated flow simulations relevant to military aircraft. *Aerospace Science and Technology*, 2021, 117, 106940.
- [28] G. H. Shah, K. Cunningham, J. V. Foster, C. M. Fremaux, E. C. Stewart, J. E. Wilborn, D. W. Pratt, Wind-tunnel investigation of commercial transport aircraft aerodynamics at extreme flight conditions, *SAE Transactions*. 2002, 386-395.
- [29] V. Klein, P. C. Murphy, Aerodynamic parameters of high performance aircraft estimated from wind tunnel and flight test data. *NASA Technical Memorandum 207993*, 1998.
- [30] J. A. Grauer, E. A. Morelli, A generic nonlinear aerodynamic model for aircraft. In *Proceedings of the AIAA Atmospheric Flight Mechanics Conference*, p. 0542, 2014.
- [31] J. A. Grauer, E. A. Morelli, Generic global aerodynamic model for aircraft, *Journal of Aircraft*. 2015, 52(1), 13-20.
- [32] S. S. Desai, Relative roles of computational fluid dynamics and wind tunnel testing in the development of aircraft, *Current Science*. 2003, 49-64.
- [33] D. Landman, J. Simpson, R. Mariani, F. Ortiz, C. Britcher, Hybrid design for aircraft wind-tunnel testing using response surface methodologies, *Journal of Aircraft*. 2007, 44(4), 1214-1221.
- [34] V. Klein, K. D. Noderer, Modeling of aircraft unsteady aerodynamic characteristics. *NASA Technical Memorandum 109120*, 1994.
- [35] K. E. Garman, K. A. Hill, P. Wyss, M. Carlsen, J. R. Zimmerman, B. H. Stirn, P. B. Shepson, An airborne and wind tunnel evaluation of a wind turbulence measurement system for aircraft-based flux measurements, *Journal of Atmospheric and Oceanic Technology*. 2006, 23(12), 1696-1708.
- [36] Z. Czyż, T. Łusiak, P. Karpiński, J. Czarnigowski, Numerical investigation of the gyroplane longitudinal static stability for the selected stabilizer angles. In *Journal of Physics: Conference Series*, IOP Publishing. 2018, Vol. 1101, No. 1, p. 012003.
- [37] S. Houston, D. Thomson, *The aerodynamics of gyroplanes*. Civil Aviation Authority 2009/02, 2010.
- [38] G. Ocokoljić, B. Rašuo, M. Kozic, Supporting system interference on aerodynamic characteristics of an aircraft model in a low-speed wind tunnel, *Aerospace Science and Technology*. 2017, 64, 133-146.

Authors' information

¹Aeronautics Faculty, Military University of Aviation, Dywizjonu 303 35, 08-521 Dęblin, Poland.

²Faculty of Mechanical Engineering, Lublin University of Technology, Nadbystrzycka 36, 20-618 Lublin, Poland.



Zbigniew Czyż graduated with a specialization in the construction and exploitation of aircraft propulsion systems at the Lublin University of Technology, Poland in 2013. He is the author of 50 reviewed papers and scientific publications, editor of 11 monographs and author of 10 chapters of monograph. He co-authored 4 patents and 16 patent applications. His main area of research involves computational fluid dynamics, heat transfer and aerodynamics. The research is aimed at the practical application and cooperation between science and enterprises. Dr Zbigniew Czyż is a staff member of the Aeronautics Faculty at the Military University of Aviation (science 2018) where he holds the position of assistant professor and of the Faculty of Mechanical Engineering at the Lublin University of Technology (since 2013) where he works as a scientist in research projects. Worker in many projects in the field of aviation propulsion systems and fluid mechanics.



Paweł Karpiński received the Master of Science degree in mechanical engineering specialization at the Lublin University of Technology, Poland in 2016. His research interest includes simulation of aircraft piston engines and computational fluid dynamics. Mr. Karpiński is a PhD student at the Faculty of Mechanical Engineering at the Lublin

University of Technology.



Krzysztof Skiba received the Master of Science degree in mechanical engineering specialization at the Lublin University of Technology, Poland in 2013. His research interest includes aircraft propulsion systems and aircraft piston engines. Mr. Skiba works as a contractor in scientific research projects at the Faculty of Mechanical Engineering at the Lublin University of

Technology.



Mirosław Wendeker is a professor at the Mechanical Engineering Faculty at the Lublin University of Technology, Poland. Professor Wendeker holds the position of the Head of the Department of Thermodynamics, Fluid Mechanics and Propulsion Systems at the Lublin University of Technology. He is a renowned technology expert with over 30 years of experience in the field of automotive, aerospace, and energy industries. Prof. Wendeker invented, tested, and implemented many advanced technologies, certified by 13 patents and awarded with a gold medal at the 2014 Geneva Inventions international conference.